

Trajectory Extending Kinetic Monte Carlo Simulations to Evaluate Pure and Gas Mixture Diffusivities through a Dense Polymeric Membrane [†]

Subhadeep Dasgupta,[‡] Arun K.S.,[‡] K. Ganapathy Ayappa,[¶] and Prabal K. Maiti^{*,‡}

[‡]*Department of Physics, Indian Institute of Science, Bangalore, 560012, India*

[¶]*Department of Chemical Engineering, Indian Institute of Science, Bangalore, 560012, India*

E-mail: maiti@iisc.ac.in

Abstract

With renewed interest in CO₂ separations, carbon molecular sieving (CMS) membrane performance evaluation requires diffusion coefficients as inputs to have reliable estimate of the permeability. An optimal material is desired to have both high selectivity and permeability. Gases diffusing through dense, CMS and polymeric membranes experience extended sub-diffusive regimes which hinders reliable extraction of diffusion coefficients from mean squared displacement data. We improve the sampling of the diffusive landscape by implementing the trajectory extending kinetic Monte Carlo (TEKMC) technique to efficiently extend MD trajectories from ns to μ s timescales. The obtained self-diffusion coefficient of pure CO₂ in CMS membranes derived from 6FDA/BPDA-DAM precursor polymer melt is found to linearly increase from $0.8 - 1.3 \times 10^{-6} \text{ cm}^2 \text{ s}^{-1}$ in the pressure range of 1 – 20 bar which supports previous experimental findings. We also extend the TEKMC algorithm to evaluate the mixture diffusivities in binary mixtures to determine the permselectivity of CO₂ in CH₄ and N₂ mixtures. The mixture diffusion coefficient of CO₂ ranges from $1.3 - 7 \times 10^{-6} \text{ cm}^2 \text{ s}^{-1}$ in binary mixture CO₂:CH₄ which is significantly higher than the pure gas diffusion coefficient. Robeson plot comparisons show that the permselectivity obtained from pure gas diffusion data are significantly lower than that predicted using mixture diffusivity data. Specifically in the case of the CO₂:N₂ mixture we find that using mixture diffusivities led to permselectivities lying above the Robeson limit highlighting the importance of using mixture diffusivity data for an accurate evaluation of the membrane performance. Combined

[†]Preprint — The Journal of Physical Chemistry B — Accepted on October 25, 2023

with gas solubilities obtained from grand-canonical Monte Carlo simulations, our work shows that simulations with the TEKMC method can be used to reliably evaluate the performance of materials for gas separations.

Introduction

Separating CO₂ from natural gas streams primarily involves the separation of CO₂ from gas mixtures. Separation technologies largely comprise solvent-based extraction techniques, cryogenic distillation, and membrane-based separations.¹ Solvent based extraction techniques, like amine filtration, exhibit long term environmental concerns regarding energy consumption, operating challenges, and emission of hazardous by-products.² Currently, industrial applications are dominated by cryogenic distillation. However, it has serious drawbacks pertaining to high energy requirements and high operating costs.³ Membrane-based gas separation offers significant advantages, due to increased stability, scalability, with potential to improve performance based on synthesis of novel materials, while being relatively hazard-free.⁴ Carbon based membranes have shown a lot of promise for effectively separating CO₂ from natural gas streams. Carbon molecular sieving (CMS) membranes are carbon-based high-performance gas separation membranes, derived from the pyrolysis of polymeric precursors in vacuum or inert atmosphere. CMS membranes present a bimodal pore-size distribution and a rich network of interconnected micropores ($\sim 0.7 - 2$ nm) and ultra-micropores (< 0.7 nm) that can differentiate between pairs of gas molecule having similar kinetic diameters.⁵⁻⁸ Similar pore network topologies are observed in a variety of other polymeric membranes, enabling one to modify membranes by varying the chemistry and processing conditions.⁹ Membrane based technologies also have the advantage of excellent gas selectivity with high gas permeability, chemical and thermal stability.^{10,11} CMS membranes show great promise in carbon capture and storage applications, with their monomer composition and choice of precursor playing an important role in determining their gas adsorption and selectivity performances.

Molecular simulations are widely used to study gas adsorption and separation processes. Grand-canonical Monte-Carlo (GCMC) simulations have been used to obtain adsorption isotherms for a variety of molecules and microporous materials such as metal organic frameworks (MOFs), zeolites and carbon based materials. These simulations are carried out under equilibrium conditions. In contrast the transport mechanism of gases inside membranes occur in non-equilibrium conditions across an applied pressure gradient between the upstream feed gas to be separated and the downstream gas. In this regard, polymeric membranes have been widely studied for effective CO₂ separations. Gas transport through dense polymer membranes are generally modelled by the sorption-diffusion mechanism.¹²⁻¹⁴ Gas molecules first adsorb in the membrane at the upstream conditions, diffuse under the influence of a chemical potential gradient, and finally desorb from the membrane at the downstream compartment. The diffusive flux of the gas molecule through the membrane is measured using its permeability,

$$\mathcal{P} = SD \tag{1}$$

where S and D are the solubility and diffusion coefficients of the gas molecule respectively in the membrane.¹⁵ High permeability values can be achieved by increasing either D or S or

both D and S . If the upstream pressure is much larger than the downstream pressure then the solubility S can be obtained from an equilibrium GCMC simulation evaluated at the thermodynamic conditions at the upstream pressure. Molecular dynamics (MD) simulations have been widely used to evaluate the diffusion coefficient, D in a variety of microporous materials.^{16–20} Due to the complex porous networks present in glassy polymeric membranes and their derivatives, there is a drastic slowing down of the dynamics of the diffusing species. As a result carrying out all-atom MD simulations to adequately sample the diffusive regime and reliably evaluate D is a computational challenge. Alternate approaches have been devised to overcome this limitation with the primary goal of evaluating the self-diffusion coefficients of slowly diffusing gas species. Thornton *et al.* presented an approximate dependence of gas diffusivity on fractional free volume of the porous media and the kinetic diameter of the gas, derived empirically from available experimental data.²¹ Bousige *et al.* analyzed the residence and relocation times of fluid in ultraconfining disordered porous materials by mapping MD simulations to mesoscopic random walks.²² Neyertz *et al.* proposed a variant of kinetic Monte Carlo (kMC), referred to as trajectory extending kinetic Monte Carlo (TEKMC).²³ The algorithm has been successfully used to calculate the diffusion coefficients of small molecules such as H₂O, O₂, N₂ in glassy polymers.^{23,24}

While assessing a given material for a particular gas separation technology both solubility and diffusion coefficients in a gas mixture need to be evaluated. The gas solubility can be obtained from mixture GCMC simulations, however evaluating diffusion coefficients of mixtures is more challenging.^{25,26} There are several reports of computing gas permeabilities in polymers, metal organic frameworks, zeolites using both pure and mixture gas data while comparing with the Robeson upper limit^{27,28} where higher selectivity is correlated with lowered permeability. These plots are used as a standard to assess the performance of newly fabricated adsorbents where the goal is to design a material with both high selectivity and permeability. There are also ongoing efforts to redefine and increase the upper limits for different materials.^{29–31} With a wide range of data available, machine learning based techniques have also been leveraged to understand and find materials that can surpass the Robeson upper bounds.³² Recent attempts to address mixture diffusivities from MD simulations showed that gas molecules tend to oscillate between adsorption sites³³ making it difficult to evaluate the long-time gas diffusivity. Since the evaluation of diffusion coefficients in mixtures is challenging several studies evaluate the permeabilities using pure component diffusion coefficients. Semi-empirical approaches which have been developed with varying degrees of success to obtain mixture diffusion coefficients from pure diffusivity data.³⁴ Lattice-based techniques have been used to compute diffusion of gases inside such variable pore structures,^{35,36} however they require various parameters which are difficult to determine. In this work, to overcome these limitations, we extend the TEKMC technique to reliably obtain mixture diffusivities of gases inside the 6F-CMSM membrane. Robeson plot comparisons are made with permeability data obtained from both pure and mixture diffusivities to highlight the limitations of using pure component diffusivity data while designing membranes for gas separation applications.

In our previous study,³⁷ we modelled CMS membranes derived from 6FDA/BPDA-DAM precursor polymer melt^{38,39} (denoted as 6F-CMSM). The molecular structures were built in close correspondence with experimental compositions using density functional theory (DFT) for optimizing the two monomeric units (pyridine and pyrrole) followed by their polymeriza-

tion using all-atom MD simulations. GCMC simulations were used to obtain gas adsorption isotherms inside the membrane for a range of pressures. Our simulated 6F-CMSM morphologies helped understand the importance of the length of carbon chains in determining density of the membrane and their accessible pore volumes, which in turn affect their adsorption performances. More details about the CMS membrane simulations can be found in our previous publication.³⁷ In continuation of our previous study, here we analyze the dynamics of the adsorbed gases through the porous networks of the 6F-CMSM. The solubility coefficients needed in this work are obtained from the previous gas adsorption isotherms under different pressures. Predicting accurate values of \mathcal{P} requires estimating both S and D for each gas component. The novelty of our work lies in using TEKMC to obtain self-diffusion coefficients of CO_2 , CH_4 and N_2 in pure gases and the multicomponent diffusivities in binary mixtures, as a function of pressure. We obtain the permeability for pure gases and binary $\text{CO}_2:\text{CH}_4$ and $\text{CO}_2:\text{N}_2$ mixtures to evaluate the membrane performance. The manuscript is organized as follows. We first discuss in detail the methodology used to perform the TEKMC steps. Next we study the variation of gas diffusivities and ultimately their permeation through the 6F-CMSM. We study the relative permeabilities of these gases in both the pure state and binary mixtures in the 6F-CMSM polymeric membrane to understand its dependence on system pressure and gas compositions. We finally present the Robeson plots for the different systems to illustrate the importance of using accurate mixture diffusion coefficients while assessing a materials capacity for separating a given gas mixture.

Method

Computational modeling and simulation

The 6F-CMSM membrane used in this work is composed from pyridinic and pyrrolic monomer units shown in Fig. 1a. These monomers polymerize to form various morphologies, among which we select the structure with closest resemblance to experimental gas adsorption isotherms as discussed in our earlier work.³⁷ The structure of CO_2 , CH_4 and N_2 molecules used are shown in Fig. 1b. The interactions involving the gas molecules are modeled using the TraPPE force fields⁴⁰ and the 6F-CMSM atoms are modelled using modified Dreiding.^{38,41} The force field values used in this work are reported in Table A1 of the Appendix. The distribution of gas molecules inside the 6F-CMSM are obtained from GCMC simulations as discussed in our earlier work. To account for the structural rearrangement of monomer constituents upon interaction with gas molecules, the 6F-CMSM is modelled as a flexible membrane. We first perform all-atom MD simulations of 6F-CMSMs along with the adsorbed gases for 20 ns duration in an NVT ensemble using LAMMPS.⁴² The temperature of the system is maintained at 308 K using a Nosé-Hoover thermostat. The coordinates of the gas molecules from the MD simulation are stored at an interval of $\tau_{MD} = 10$ ps. Fig. 1c shows a snapshot from our all-atom MD simulation of 6F-CMSM loaded with CO_2 corresponding to 20 bar pressure. The porous nature of the membrane for different cross-sections along the bulk of the membrane is also visible from the simulation snapshot.

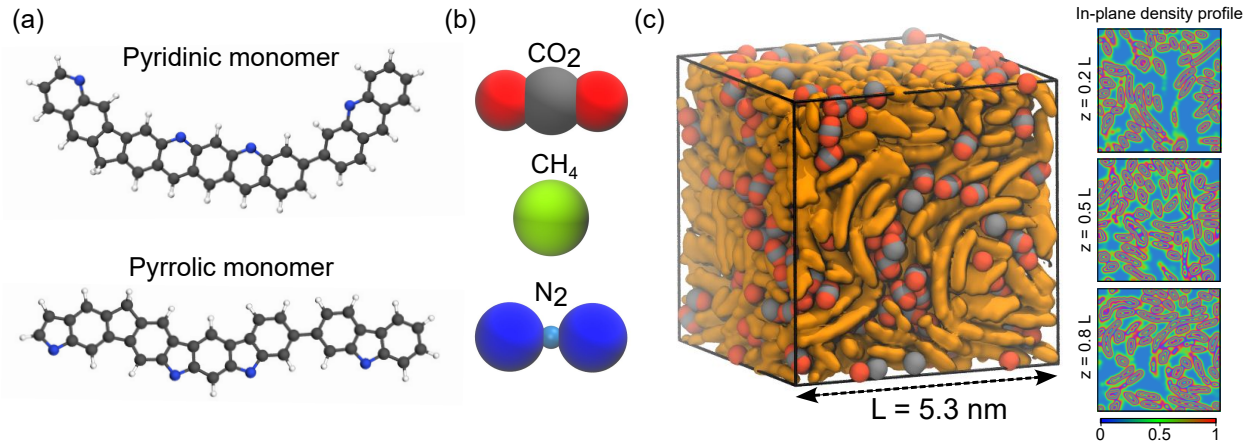


Figure 1: (a) Atomic structures of pyridinic and pyrrolic monomer fragments that cross-link and polymerize to form the derived 6F-CMS membrane. Gray denotes carbon, blue denotes nitrogen, and white denote hydrogen atoms (b) Atomic structure for the three gases considered in this work based on the TraPPE force field.⁴⁰ Three-site CO₂ is modelled with two oxygen (red) and one carbon (gray) atoms. CH₄ is represented with united atom model, having a single bead (green). The three site N₂ with two nitrogen atoms (blue) and one fictitious centre of mass bead (cyan). (c) Snapshot showing the derived 6F-CMSM containing adsorbed CO₂ in the pores, corresponding to $T = 308$ K and $P = 20$ bar. The surface of the cross-linked monomers are colored orange. Shown in the right are in-plane density profiles for three cross-sections. The blue regions represent the pores and green to red regions denote presence of 6F-CMSM atoms. The difference in porous structure across the z -plane indicate formation complex network pathways along the bulk of the 6F-CMSM. These interconnected pores govern the dynamics and diffusion of gases inside the 6F-CMSM.

Implementing kinetic Monte Carlo

The simulation box is uniformly divided into voxels of grid size (d_{grid}) along x , y , and z directions. Each voxel is identified by a single index, spanning from 1 to $n_{voxel} = (L/d_{grid})^3$, for a cubic simulation box having length L on each side. All gas molecules are mapped from their real-space (x, y, z) coordinates to their respective voxel indices. The trajectories of the gas molecules from the MD simulations are used to compute the transition probability matrix (π_{ij}) required as input for the TEKMC simulation. We define the probability of transition between voxels i and j , given that the gas is in voxel i as,

$$\pi_{ij} = \frac{N_{ij}}{N_i} \quad (2)$$

where N_{ij} is the number of transitions between voxels i and j and N_i is the number of times the gas molecule visits voxel i . Since the transition probability matrix is constructed from the all-atom MD trajectories, π_{ij} implicitly takes into account all the gas-gas and gas-membrane interactions. The probability matrix is symmetrized to maintain detailed balance, such that

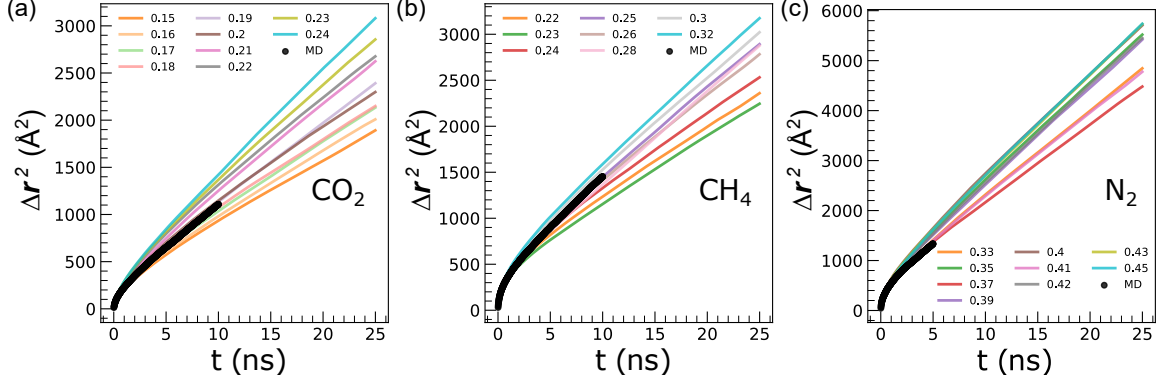


Figure 2: Mean squared displacement (Δr^2) of (a) CO_2 , (b) CH_4 and (c) N_2 , inside 6F-CMSM at a temperature of 308 K and 20 bar pressure. The thick black line shows the values obtained from the all-atom MD simulations. The finer colored lines show the values obtained from 50 ns TEKMC simulations for different values of d_{grid} (nm). The values of d_{grid} are tuned to obtain an MSD having least mean squared error *w.r.t.* the values obtained from MD simulation.

$\pi_{ij} = \pi_{ji}$, which is equivalent to

$$N_{ij} = N_{ji} = (N'_{ij} + N'_{ji})/2 \quad (3)$$

where N'_{ij} and N'_{ji} are the recorded number of transitions from voxel i to j and j to i respectively. Voxels with $\pi_{ii} = 0$ indicate regions inside the simulation box where the atoms of the CMS molecules are located. The values of (π_{ii}) for CO_2 , CH_4 and N_2 for 1 bar and 20 bar pressures are shown in Fig. A1 of the appendix. In case of binary gas mixtures, π of each component is obtained from the trajectory of that component. The interaction between two components changes the probability distribution from the pure gas system, shown in Fig. A2 of the appendix for 20 bar pressure. From conservation of number of particles, we have the condition $\sum_j \pi_{ij} = 1, \forall i$. For each kMC move, a walker is placed randomly in one of the visited voxels i such that $\pi_{ii} \neq 0$. The voxel j that the walker visits from i is determined from the sum, $\sigma(j') = \sum_1^{j'} \pi_{ij}$. The destination voxel is identified to be $j = j'$ when $\sigma(j') \geq r$ is just satisfied, where r is a random number drawn from a uniform distribution. A total of 5000 random walkers are inserted for each simulation and the time associated with each kMC step is τ_{kMC} . The trajectories of these random walkers are mapped back from the voxel index to the real space coordinates and their average mean squared displacement (MSD) is determined.

Table 1: Optimum values of d_{grid} (nm) corresponding to lowest MSE between MSD obtained from TEKMC and MD simulations for the three gases.

P (bar)	0.1	0.6	1	6	10	15	20
CO_2	0.41	0.32	0.22	0.19	0.20	0.20	0.20
CH_4	0.61	0.42	0.34	0.30	0.32	0.24	0.25
N_2	0.60	0.55	0.47	0.45	0.44	0.35	0.33

Optimization to obtain diffusion and permeability

The optimal values of τ_{MD} and d_{grid} combinations first needs to be determined for obtaining the correct MSD from the TEKMC simulation. Different techniques can be used to obtain the time interval between two successive kMC steps, τ_{kMC} .⁴³ We follow the procedure prescribed by Neyertz *et al.* where $\tau_{kMC} = \tau_{MD}$ ($= \tau$). Fig. 2 illustrates the values of MSD obtained from all-atom MD and TEKMC simulations for CO₂, CH₄ and N₂ at 20 bar pressure. For a diffusing particle the MSD, $\langle \Delta \mathbf{r}(t)^2 \rangle \propto t^\alpha$. The value of the exponent α from the MSD data obtained from MD simulations lies in the range of 0.6 \sim 0.8 indicating the sub-diffusive nature of the diffusing molecule in the polymeric membrane. In the diffusive regime where the value of $\alpha \simeq 1$, the diffusivity is obtained from the Einstein relation,

$$D = \lim_{t \rightarrow \infty} \frac{1}{6t} \langle \Delta \mathbf{r}(t)^2 \rangle = \lim_{t \rightarrow \infty} \frac{1}{6t} \langle [\mathbf{r}(t + t_0) - \mathbf{r}(t_0)]^2 \rangle \quad (4)$$

where $\langle \dots \rangle$ represent averages over all particles, and shifted time origins (t_0). The TEKMC simulations enable us to access the Brownian regime for restricted diffusing molecules which predominantly sample the sub-diffusive regime during the small timescale of MD simulations. In order to determine the optimal value of d_{grid} we used the lowest mean squared error (MSE) between MSDs obtained from the MD simulation and that obtained from 100 ns TEKMC simulations. The optimum values of d_{grid} for the different cases considered are shown in Table 1. To determine the diffusion coefficients we carry out additional TEKMC simulations for three different d_{grid} values, which include the optimal d_{grid} (Table 1) as well as simulations at $d_{grid} \pm 0.01$ nm. For these three different values of d_{grid} , random walks are performed up to 5 μ s to ensure all gases attain the Brownian diffusion regime and the reported values of D are an average over these TEKMC simulations. The in-house TEKMC code developed in this study was validated by reproducing the diffusivity of bulk water and is discussed in section of the appendix. From TEKMC, we obtain diffusion coefficient of SPC/E water to be $2.47 \pm 0.15 \times 10^{-5} \text{ cm}^2 \text{ s}^{-1}$ at 300 K, in agreement to literature^{44,45}. The algorithm is generic and can be used for other systems where such kMC algorithms are applicable. The solubility coefficient of the i^{th} gas species (S_i), in a membrane is the ratio between its volumetric loading $V_{L,i}$ and its partial pressure p_i at a constant temperature,⁴⁶

$$S_i = \frac{V_{L,i}}{p_i} \quad (5)$$

The adsorption isotherm is expressed in terms of the volumetric loading,

$$V_{L,i} = \frac{N_i(T, P)}{V_{CMS}} \frac{k_B T_{STP}}{P_{STP}} \quad (6)$$

where $N(T, P)$ is the number of gas molecules adsorbed in the 6F-CMSM membrane at temperature T and pressure P , V_{CMS} is the volume of the 6F-CMSM membrane, k_B is the Boltzmann constant, T_{STP} and P_{STP} correspond to standard temperature and pressure respectively. The equilibrated values of V_L were obtained using the Peng-Robinson equation of state⁴⁷ implemented in RASPA,⁴⁸ detailed in our previous work.³⁷ The solubility coefficients can be estimated accurately using the above equations, ultimately allowing us to compute

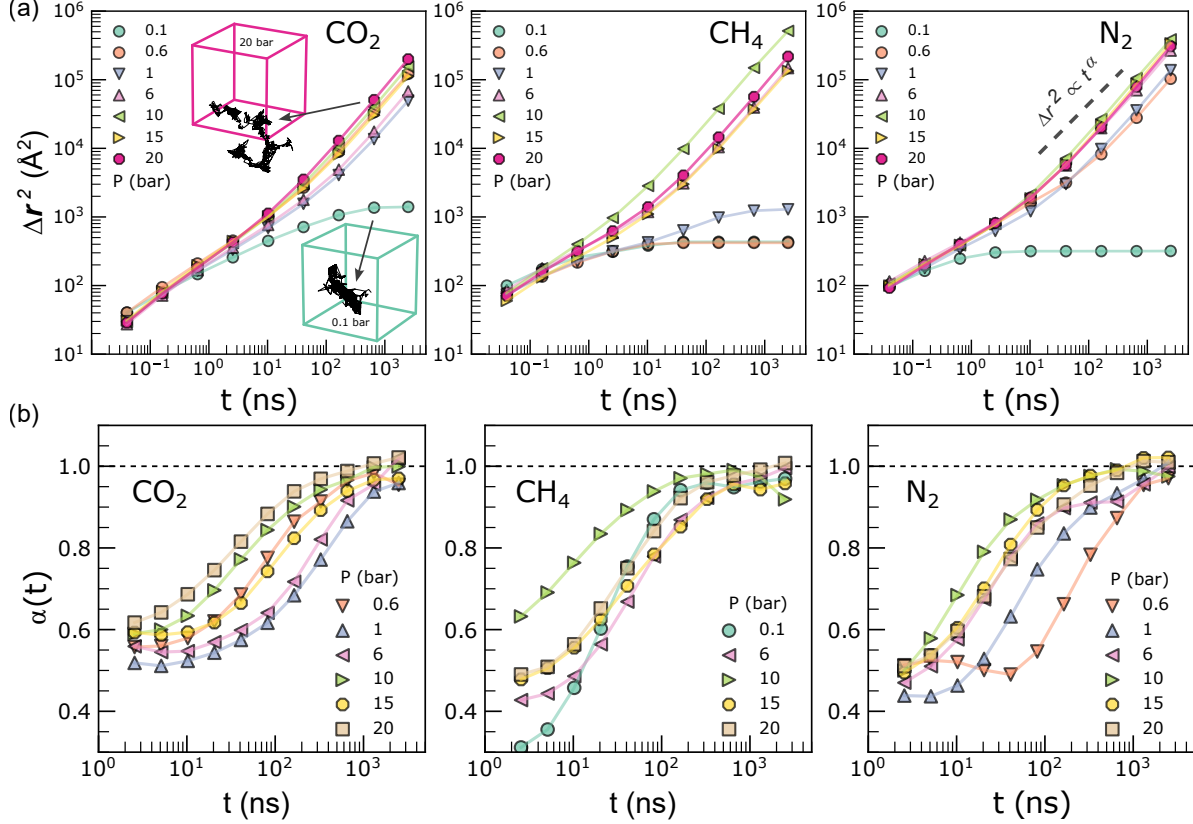


Figure 3: (a) MSD (Δr^2) versus time for different gases CO_2 , CH_4 , and N_2 . The dynamics of the gas molecules vary significantly depending on the system pressure (indicated by different colors shown in legend). The inset shows two sample, unwrapped trajectories of a walker representing CO_2 molecules inside 6F-CMSM at 0.1 and 20 bar pressures obtained from kMC. (b) The growth of MSD exponent (α) versus time for the three gases is presented for systems that attain the Brownian regime successfully. The dashed line shows the reference level of $\alpha = 1$. The time taken to reach $\alpha = 1$ decreases with increasing pressure.

their corresponding permeabilities.

Results and discussion

Gas dynamics inside 6F-CMSM

Fig. 3a shows the averaged MSD (Δr^2) of CO_2 , CH_4 and N_2 for the entire range of system pressures obtained from 5 μs TEKMC simulations and the corresponding values of the exponent α are illustrated in Fig. 3b. The time taken to attain the Brownian regime for the three gases is significantly higher at low pressures compared to the time taken at higher pressure. We observe a slow growth of the exponent towards $\alpha = 1$ and the Brownian regime is observed above a sampling time of 1 μs . The inset in Fig. 3a illustrates two representative trajectories for CO_2 molecules corresponding to 0.1 and 20 bar pressures. At low pressures (0.1 bar) gas molecules remain trapped in higher energy adsorption sites restricting displace-

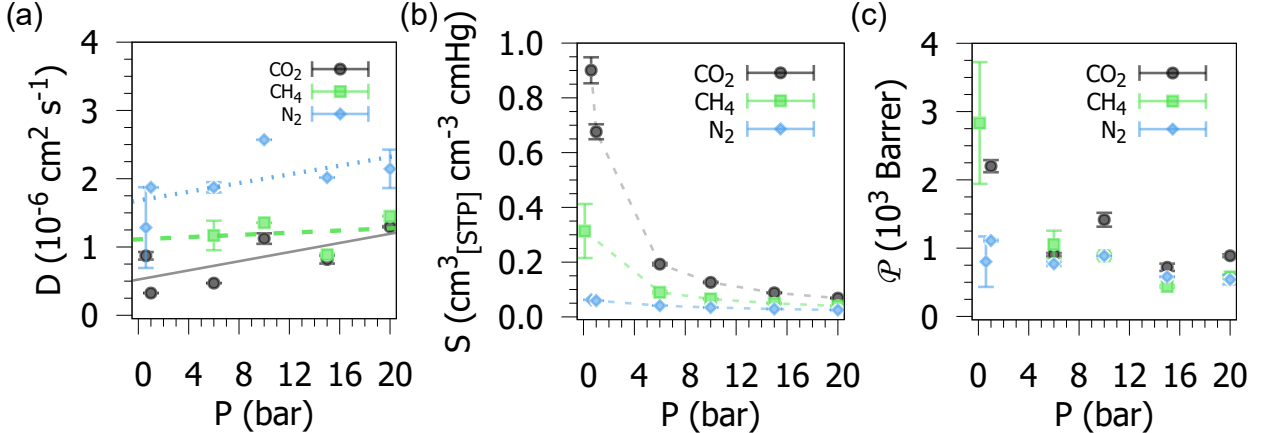


Figure 4: Dependence of (a) self-diffusion coefficient, D , (b) solubility coefficient, S , and (c) permeability, \mathcal{P} of pure CO_2 , CH_4 , N_2 adsorbed inside 6F-CMSM for increasing pressure P at $T = 308$ K. The data shown are averaged over independent kMC simulations using three best grid sizes for each pressure point.

ments to a small region of the CMS membrane and results in a sub-diffusive nature of the MSD ($\alpha < 0.7$) even after $5 \mu\text{s}$. At higher pressures, a distinct crossover from sub-diffusive to diffusive regimes is observed. We note that at higher pressure, increased gas uptake results in swelling of 6F-CMSM giving rise to flexible permeation pathways.³⁷

The diffusion coefficients obtained from the Brownian regimes, ($\alpha \simeq 1$), for different pressures are shown in Fig. 4a. In literature, the experimentally reported value of D for CO_2 inside 6F-CMSM derived from 6FDA/BPDA-DAM pyrolysed at 550°C is $1.32 \times 10^{-6} \text{ cm}^2 \text{ s}^{-1}$.⁴⁹ Our calculated value of D_{CO_2} is in excellent agreement with the experimental value. From the values obtained in Fig. 3, the estimated timescale for obtaining diffusive regime at pressure $P = 20$ bar is around 500 ns for CO_2 . For cross-validation against all-atom MD results, we performed an additional all-atom MD simulation for 500 ns . The diffusion coefficient from the all-atom MD $\sim 1.23 \times 10^{-6} \text{ cm}^2 \text{ s}^{-1}$. Both the experimental and all-atom MD values are close to the converged value obtained using TEKMC. This remarkable agreement further allows us to conclude that the algorithm can successfully extrapolate short MD results to longer duration and can be successfully used for computing diffusion of confined gas molecules. We also observe that a sufficient number of percolating pathways are required during the atomistic MD simulation in order to adequately access all possible pores available for the gas molecules to diffuse through. From the dependence of D on P , in Fig. 4a we observe a linear increase in the diffusivities of all three gases inside the 6F-CMSM as a function of pressure. The loading-dependent diffusion coefficients have been observed for hydrocarbons in metal organic frameworks¹⁷ which lead to structural changes of the adsorbing framework.⁵⁰ There is a monotonic increase of D in the pressure range studied for all gases, which is non-trivial and to the best of our knowledge not reported earlier for CMS membranes. We observe that N_2 diffuses faster than CO_2 inside 6F-CMSM which is similar to the diffusive nature inside zeolites reported in literature.¹⁸

Solubility and permeability of pure gases

The solubilities, (S) of CO_2 , CH_4 , and N_2 versus pressure for 6F-CMSM corresponding to temperature 308 K using the values of V_L from our previous study of gas uptake in 6F-CMSM³⁷ and calculated using Eq. 5 are shown in Fig. 4b. The values of S for CO_2 are the highest followed by CH_4 . N_2 solubilities are the lowest and independent of pressure. We observe a monotonic decrease in the solubility coefficient with increase in pressure for all gases inside the 6F-CMSM. Permeability (\mathcal{P}) is then obtained using Eq. 1 in units of Barrer and shown in Fig. 4c. In general, the permeability values for CO_2 are the highest when compared with CH_4 and N_2 . We also observe that the permeability decreases with pressure with the most noticeable variation seen in CO_2 and CH_4 , the effect is less pronounced for N_2 . The linear growth of D with P , signifies that any variation in \mathcal{P} is strongly dominated by S .

Permselectivity in binary gas mixtures

In order to understand the relative permeability of different gases inside 6F-CMSM, we also compute the permselectivity ($\alpha_{\mathcal{P}}$) of CO_2 in binary gas mixtures of $\text{CO}_2:\text{CH}_4$ (50 : 50 and 10 : 90) and $\text{CO}_2:\text{N}_2$ (20 : 80). The permselectivity in gas mixture is given by,

$$\alpha_{\mathcal{P}} = \frac{\mathcal{P}_X}{\mathcal{P}_Y} \quad (7)$$

where X denotes CO_2 and Y denotes CH_4 or N_2 depending on the composition of gas mixture. The diffusion coefficient of gas molecules are influenced by their interactions with the membrane as well as with neighboring gas molecules. Consequently, the diffusion coefficient of each component in a mixture deviates from the corresponding pure gas diffusion coefficients. The deviation is non-trivial and there is an on-going effort to understand multicomponent gas diffusion in different adsorbing frameworks.^{16,18,19,51,52} To address this challenge, we extended the TEKMC simulations to gas mixtures of different compositions. The probability matrix for the binary gas mixture is created by tracking the positions of individual gas species during the MD runs as was done for the pure single component system described earlier. We performed separate TEKMC simulations for each species in the binary gas mixture system, to obtain the corresponding mixture diffusion coefficients for each component in the mixture. The TEKMC optimization was also carried out independently for each mixture at different pressures, to obtain the diffusivities. This data is obtained from 5 μs long TEKMC simulations and the diffusivities were computed from the MSD data over 2.5 μs to sample the Brownian diffusive regime (Fig. A3). For the binary mixtures, the permeability \mathcal{P}_i for the i^{th} component is obtained from the corresponding solubility S_i . S_i values are obtained using Eq. 5, from binary mixture GCMC simulations reported in our previous work.³⁷ The corresponding values of D_i , S_i and \mathcal{P}_i for the different gas mixtures are given in Table 2. The variations of the diffusive exponent α for the mixtures are illustrated in Fig. A3 of the appendix. We observe that the diffusivities of CO_2 , CH_4 , and N_2 in their binary mixtures deviate significantly from the pure component values. D_{CO_2} is greater in majority of the binary mixtures when compared to diffusivity of pure CO_2 for a given pressure value reflecting the altered energy landscape for CO_2 in the mixture. The diffusivity of both CH_4

Table 2: Diffusion coefficients, solubility and permeability of each species for different binary gas mixtures inside 6F-CMSM.

P (bar)	D_i (10^{-6} cm ² s ⁻¹)		S_i (10^{-2} cm ³ _[STP] cm ⁻³ cmHg)		\mathcal{P}_i (10^3 Barrer)	
	CO ₂ : CH ₄ (50 : 50)					
	CO ₂	CH ₄	CO ₂	CH ₄	CO ₂	CH ₄
4	1.34 ± 0.12	0.78 ± 0.26	39.96 ± 3.00	4.85 ± 0.76	5.34 ± 0.61	0.38 ± 0.14
6	1.65 ± 0.20	0.50 ± 0.13	29.78 ± 2.22	3.59 ± 0.56	4.91 ± 0.69	0.18 ± 0.06
10	3.35 ± 0.14	4.75 ± 0.83	20.09 ± 1.49	2.35 ± 0.38	6.72 ± 0.58	1.12 ± 0.27
15	3.42 ± 0.44	4.24 ± 0.78	14.36 ± 1.03	1.68 ± 0.26	4.91 ± 0.72	0.71 ± 0.11
20	7.02 ± 0.67	13.55 ± 0.78	11.22 ± 0.78	1.27 ± 0.20	7.88 ± 0.93	1.73 ± 0.28
	CO ₂ : CH ₄ (10 : 90)					
	CO ₂	CH ₄	CO ₂	CH ₄	CO ₂	CH ₄
4	2.07 ± 0.07	0.73 ± 0.26	78.28 ± 28.29	8.55 ± 0.80	16.16 ± 5.87	0.62 ± 0.23
6	5.87 ± 0.35	7.25 ± 0.52	61.31 ± 19.76	6.61 ± 0.56	35.99 ± 11.80	4.80 ± 0.53
10	5.4 ± 0.43	9.92 ± 0.53	43.21 ± 10.66	4.62 ± 0.3	23.31 ± 6.04	4.59 ± 0.39
15	2.12 ± 0.20	1.47 ± 0.13	32.34 ± 7.76	3.41 ± 0.22	6.87 ± 1.77	0.50 ± 0.06
20	7.41 ± 0.36	12.90 ± 0.82	26.01 ± 5.64	2.70 ± 0.16	19.27 ± 4.28	3.48 ± 0.30
	CO ₂ : N ₂ (20 : 80)					
	CO ₂	N ₂	CO ₂	N ₂	CO ₂	N ₂
4	1.50 ± 0.12	3.00 ± 0.45	71.91 ± 7.66	2.03 ± 0.49	10.77 ± 1.44	0.61 ± 0.17
6	2.14 ± 0.19	2.80 ± 0.16	56.13 ± 5.41	1.58 ± 0.35	11.98 ± 1.56	0.44 ± 0.10
10	2.44 ± 0.16	2.11 ± 0.19	39.59 ± 3.53	1.14 ± 0.23	9.65 ± 1.07	0.24 ± 0.05
15	1.44 ± 0.08	2.27 ± 0.22	29.57 ± 2.47	0.86 ± 0.02	4.26 ± 0.43	0.20 ± 0.04
20	2.35 ± 0.16	3.18 ± 0.22	23.81 ± 2.00	0.67 ± 0.01	5.59 ± 0.60	0.21 ± 0.04

and N₂ are higher than that of CO₂ particularly at higher pressures. The difference in the mixture diffusivities of the two species is higher for CH₄ than N₂. However, the high adsorption of CO₂ onto 6F-CMSM leads to significantly higher S_{CO_2} which in turn results in a greater increase for \mathcal{P}_{CO_2} when compared with CH₄ and N₂. We also note a decrease in the diffusivities for the CO₂ : CH₄ (10 : 90) at a pressure of 15 bar, however the reason for this particular deviation is not completely understood as the MSD data was well within the diffusive regime for both species.

Fig. 5a shows the Robeson plots for different mixtures where we have used the solubility mixture data with pure component diffusivity values to obtain the permeabilities. In Fig. 5b mixture data (Table 2) was used for both the solubilities and diffusivities. The Robeson upper limit for different CO₂:CH₄ and CO₂:N₂ are plotted for comparison.²⁷ Upon comparing Fig. 5a, b, we first note that both α_P and \mathcal{P} increase while using values for S_i and \mathcal{P}_i computed from mixture data. Using pure component D_i values for the Robeson plot results in a lowering of the corresponding values leading to underpredicting the performance of a given material. In Fig. 5a we observe a single point for the CO₂:N₂ (20 : 80) mixture that lies above the Robeson limit. This point corresponds to the lowest pressure of 0.6 bar for which we did not evaluate the corresponding mixture diffusivities. Interestingly we observe that the data for the CO₂:N₂ (20 : 80) mixture lies at or above the Robeson upper limit when mixture diffusivity data is used (Fig. 5b). Similar trends are observed for the CO₂:CH₄ (10 : 90) mixture as well as the CO₂:CH₄ (50 : 50). The increase in \mathcal{P}_i for CO₂ is primarily due to the increase in the diffusivities of CO₂ in the mixtures compared to the pure gas diffusivities. The increased permselectivities, α_P are due to a higher diffusivity

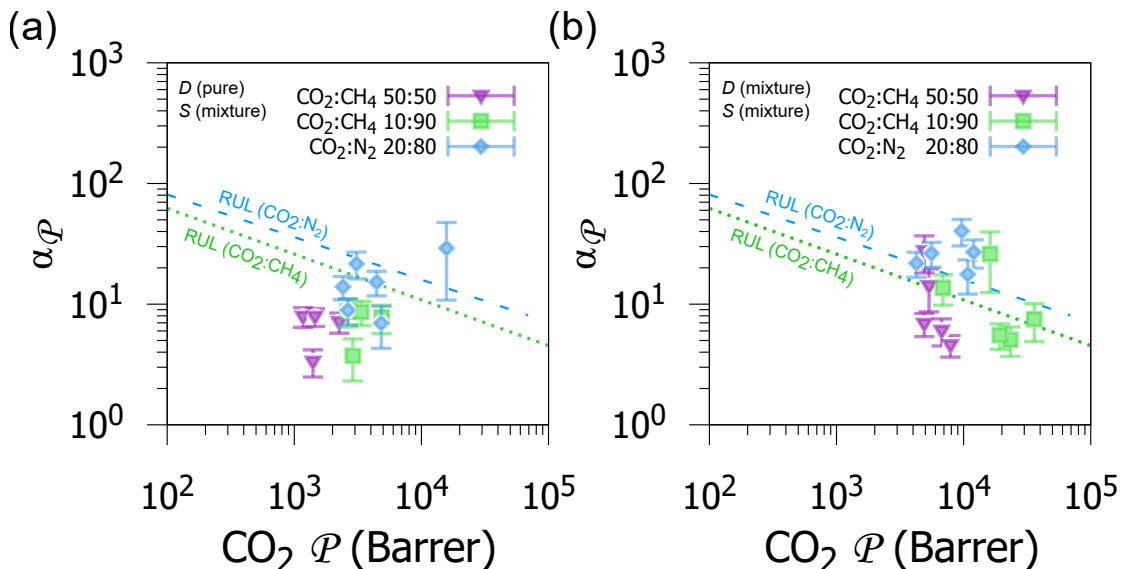


Figure 5: (a) Permselectivity ($\alpha_{\mathcal{P}}$) calculated using diffusion (D) from pure gas simulations and solubility (S) from binary gas mixtures inside 6F-CMSM. (b) $\alpha_{\mathcal{P}}$ calculated using both D and S from binary gas mixtures. \mathcal{P} and $\alpha_{\mathcal{P}}$ from computed from binary gas simulations are higher than that from pure gas simulations. The dashed lines correspond to the Robeson upper limit (RUL) for different gases.²⁷ $\alpha_{\mathcal{P}}$ obtained from mixture simulations are significantly higher from pure simulation values.

ratio obtained with mixture diffusivities.

Our results indicate that using values of single component gas diffusivities can lead to an underestimation of the true permselectivity of a membrane. Hence obtaining accurate estimates of the diffusivity in both experiments and simulations are needed in order to assess the separation performance of a given material. This will also facilitate a better understanding of the Robeson upper limits possessed by different membranes synthesized in the laboratory as well as from in silico predictions using MD simulations and machine learning based predictions.^{30,32} We finally point out that although we have observed these trends for a specific adsorbent, in this case the 6F-CSM membrane, a similar analysis would be required to assess the generality of the trends observed in this study.

Conclusion and outlook

In this work we obtained the permeability of CO₂, CH₄ and N₂ gases inside a 6F-CMS membrane for different pressure conditions using multiscale computational techniques, namely all-atom molecular dynamics followed by trajectory extending kinetic Monte Carlo simulations. The dynamics of adsorbed gas molecules inside the membrane is usually retarded, leading to sub-diffusive mean squared displacements in the timescales of typical all-atom molecular dynamics simulations. To sample the diffusive dynamics regime, the TEKMC algorithm enables us to extend all-atom MD trajectories to 5 μ s timescales where the diffusive limit can be reliably sampled. The constructed transition probability matrices also

helps us understand accessible and inaccessible regions of the complex pore networks in the membrane. In a distinct departure from earlier works we extend the TEKMC simulations to obtain diffusion coefficients of gas mixtures. To our knowledge this is the first time that mixture diffusivity data has been obtained using this method. For pure components CO_2 , N_2 and CH_4 , We report a linear increase in the gas diffusivity confined in the 6F-CMSM matrix with increasing in pressure. Conversely both the solubility and permeability of the gases are found to decrease with pressure.

We make a detailed comparison of the permselectivity using both pure component and mixture diffusivity data in the 6F-CMS membrane to assess the extent of deviations observed when pure component diffusivity data are used in lieu of mixture diffusivities. The implementation of the TEKMC algorithm is available as a package on request. Gas solubility data are calculated using previous GCMC mixture simulations.³⁷ CO_2 diffusivities in both CH_4 , and N_2 mixtures in the 6F-CMS membrane were found to be higher than the pure component values. This leads to a significant increase in both the permselectivity and permeabilities with the use of mixture diffusivities on the Robeson plots, with data lying at or above the Robeson upper limit for the $\text{CO}_2:\text{N}_2$ (20 : 80) mixtures. Our analysis indicates that for the $\text{CO}_2:\text{CH}_4$ and $\text{CO}_2:\text{N}_2$ mixtures investigated in this study, pure component diffusivities underestimates the membrane performance by varying amounts. Our findings emphasizes the importance of obtaining accurate mixture diffusivity data while designing membranes for a given separation process. Coupled with GCMC and combined MD and TEKMC simulations our study provides a complete in silico framework that can be routinely used to assess the performance of membranes for gas separation processes. We restricted our analysis to the TEKMC study of self-diffusion coefficients in order to determine the gas permeabilities for the Robeson plots to assess separation performance in the polymeric membranes. The TEKMC analysis can potentially be extended to obtain the mutual diffusion coefficients, determined from cross correlations between different species in the mixture.⁵³ Correlations between species in a mixture are a function of the pore size, gas loading and interactions between the gas and the surface. A detailed analysis is needed to fully assess the determination of transport diffusivities while evaluating the gas permeabilities in polymeric membranes.

Data Availability Statement

The data underlying this study are available on request. The code is openly available at <https://github.com/PKMLab/tekmc>.

Acknowledgement

The authors thank the Department of Science and Technology, India for funding and providing computational resources.

Appendix

Force field parameters

The interactions involving the gas molecules are modeled using the TraPPE force fields⁴⁰ and the 6F-CMSM atoms are modelled using modified Dreiding.^{38,41} The values are shown in Table A1.

Table A1: Parameters for LJ potential and atomic charges for gas molecules and 6F-CMSM.

Molecule	Site	σ (Å)	ϵ (K)	q (e)	Bond length (Å)
CMS	H	1.65	7.65	0.056	–
	N_R	3.26	38.95	–0.617	–
	C_3	3.47	47.86	0.059	–
	C_R_r	3.47	47.86	–0.078	–
	C_R	3.47	47.86	–0.078	–
CH ₄	CH ₄	3.73	148.0	–	–
CO ₂	C	2.80	27.0	0.70	C – O = 1.16
	O	3.05	79.0	–0.35	
N ₂	N	3.31	36.0	–0.482	N – N = 1.1
	COM	0.0	0.0	0.964	

Validation of TEKMC algorithm using bulk water simulations

We performed a fully atomistic MD simulation of the bulk water system consisting of 800 SPC/E⁵⁴ water molecules using LAMMPS. Initial positions of water molecules were randomly assigned inside the MD box with a constraint that all of them are separated by a threshold distance greater than the bond length of water. Periodic boundary conditions were enforced in all directions. The bulk water system was energetically minimized to remove bad contacts. The minimization comprised of 500 steps of steepest descent followed by 500 steps of conjugate gradient. After the energy minimization, the system was heated to 300 K in steps of 30 K, each for 10 ps, using a Langevin thermostat.⁵⁵ The system is next simulated in an NPT ensemble so that the system attains appropriate density at 1 atm pressure. During the NPT run of 1 ns at 300 K temperature and 1 atm pressure, the density of the system reaches equilibrium by varying the MD box boundaries. To maintain a constant pressure of 1 atm, Nosé-Hoover barostat was used with a coupling constant of 2 ps. Finally, we perform a production run for 1 ns in an NVT ensemble. Nosé-Hoover thermostat^{56,57} with a heat bath coupling constant of 1 ps was used to maintain a constant temperature during the production run. The velocity-Verlet scheme was used to do the MD integration with an integration time step of 1 fs. The OH bond was constrained using the SHAKE⁵⁸ algorithm. To compute the long-range Coulomb potential, particle-particle particle-mesh

Ewald summation method (PPPM)⁵⁹ was used with a tolerance of 10^{-5} . The trajectory of water molecules was dumped every 10 ps.

The TEKMC algorithm uses trajectories obtained from the production run to extend the MSD to a longer time scale. Trajectories obtained from the NVT simulation are used by the TEKMC algorithm to extend the MSDs to larger time scales. The timestep between the MD frames analyzed by TEKMC is 10 ps. Hence, the timestep between steps of the random walk is 10 ps. From the 1 ns NVT simulation of SPC/E water, the transition probability matrix is estimated during the first stage of the TEKMC algorithm. We perform 3000 random walks for various grid sizes up to 3 ns and tune the grid size to match with the MSD of MD simulation.

Random walks of TEKMC were extended till 100 ns for these grid sizes. MSD and diffusion coefficient till 0.5 ns obtained from the MD simulation are also shown. Grid size of 0.28 nm best matches the MD data (having the lowest MSE). The exponent α is 1.0, indicating that MSD is linear with time and SPC/E water follows Fickian diffusion in this time scale. From TEKMC, we obtain diffusion coefficient of SPC/E water to be $2.47 \pm 0.15 \times 10^{-5} \text{ cm}^2 \text{ s}^{-1}$, in good agreement to the literature value of $2.75 \times 10^{-5} \text{ cm}^2 \text{ s}^{-1}$.⁴⁴ The diffusion coefficient of bulk water obtained from simulations is subject to finite size effects based on the size of the box and number of molecules.⁴⁵ The main goal of our validation was to reproduce the MD obtained MSD by tuning d_{grid} during TEKMC. Once validated, our main focus is on the gas diffusivity inside the ultramicropores. Diffusion in the polymeric membrane is related to the inherent pore size distribution in the membrane which could be influenced by finite size effects. We point out that the polymeric membranes used in this study have been prepared by using extensive compression and decompression cycles which has shown to reproduce the experimental pore size distribution and adsorption isotherm for this system.³⁷ The finite size corrected diffusivities may also be obtained by a suitable further tuning of d_{grid} . The self-diffusion coefficient of pure water has been measured to be $2.3 \times 10^{-5} \text{ cm}^2 \text{ s}^{-1}$ at 298 K from experimental techniques like diaphragm-cell technique⁶⁰ or the pulsed-gradient spin echo (PGSE) NMR method.⁶¹

Probability distribution of gases used for performing TEKMC

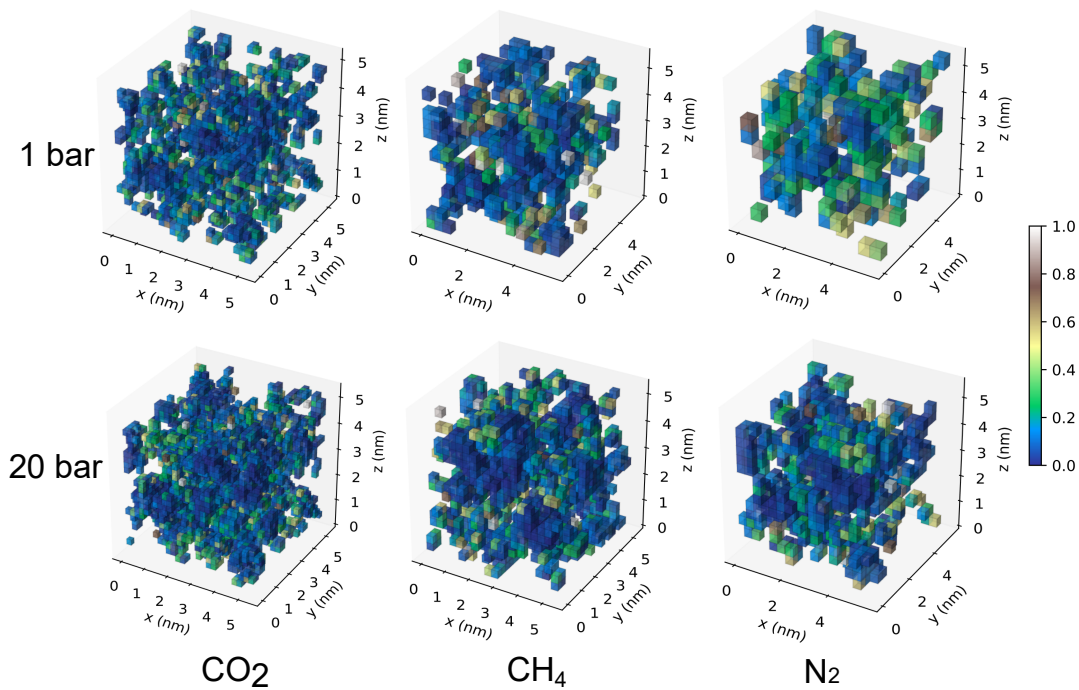


Figure A1: Probability of survival in a voxel for pure gas systems at two pressure values. The size of the voxel corresponds to the optimum d_{grid} per system.

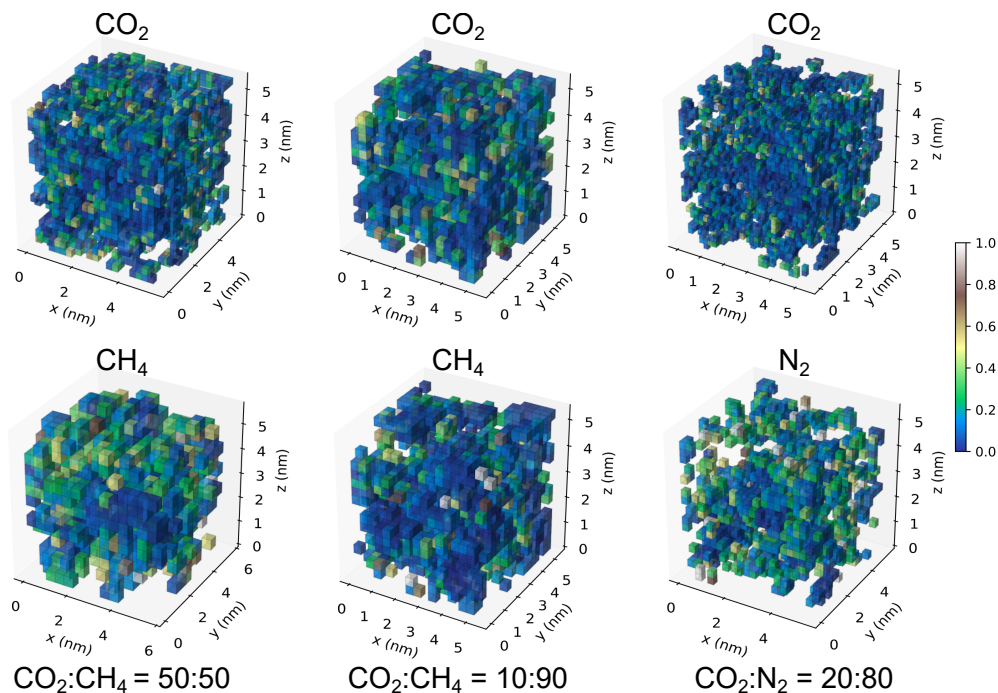


Figure A2: Probability of survival in a voxel for different binary gas mixture systems at 20 bar pressure.

Binary component diffusion inside 6F-CMSM

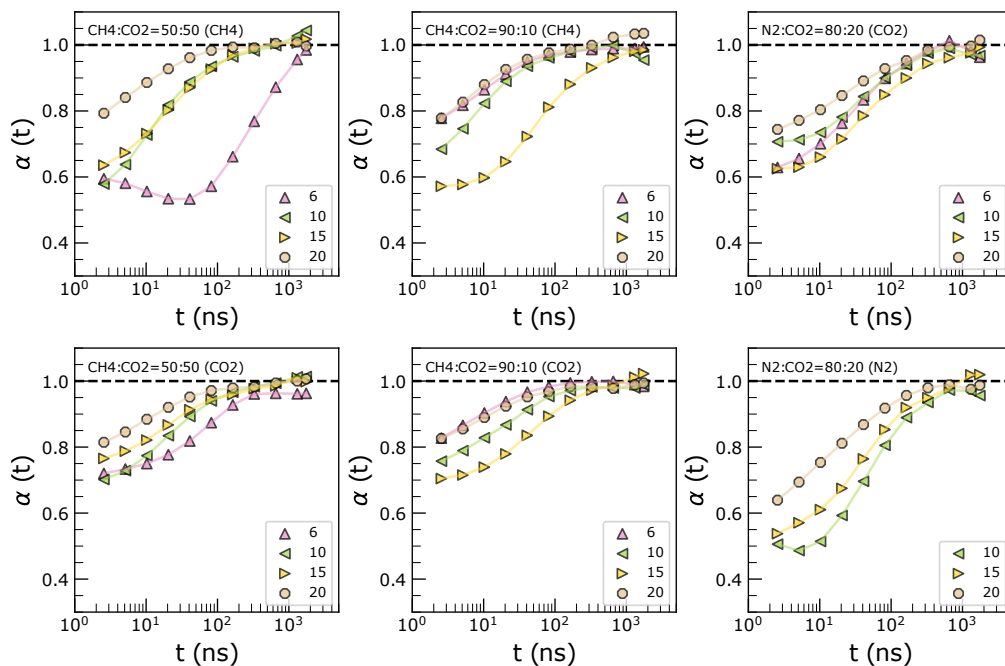


Figure A3: Time series of MSD exponent (α) for the different binary mixture systems studied. The legend shows different pressure, P (bars).

We perform MD simulations of binary gas mixtures inside 6F-CMSM corresponding to different pressure conditions. The obtained trajectories are then extended till 5 μ s to obtain mixture diffusion coefficients of the different gases. We find the diffusivities are significantly different in the mixture compared with the pure gases shown in the main accompanying text. The diffusivity of CO₂ is comparable to CH₄ or N₂ only for low pressures. The diffusivity is also affected by the molar ratio of the mixtures.

References

- (1) Carta, M. In *Encyclopedia of Membranes*; Drioli, E., Giorno, L., Eds.; Springer Berlin Heidelberg: Berlin, Heidelberg, 2015; pp 1–3.
- (2) Nielsen, C. J.; Herrmann, H.; Weller, C. Atmospheric Chemistry and Environmental Impact of the Use of Amines in Carbon Capture and Storage (Ccs). *Chemical Society Reviews* **2012**, *41*, 6684–6704.
- (3) Bhatta, L. K. G.; Subramanyam, S.; Chengala, M. D.; Olivera, S.; Venkatesh, K. Progress in hydrotalcite like compounds and metal-based oxides for CO₂ capture: a review. *Journal of Cleaner Production* **2015**, *103*, 171–196, Carbon Emissions Reduction: Policies, Technologies, Monitoring, Assessment and Modeling.
- (4) Koros, W. J. Evolving Beyond the Thermal Age of Separation Processes: Membranes Can Lead the Way. *Aiche Journal* **2004**, *50*, 2326–2334.
- (5) Kamath, M. G.; Itta, A. K.; Hays, S. S.; Sanyal, O.; Liu, Z.; Koros, W. J. Pyrolysis End-Doping To Optimize Transport Properties of Carbon Molecular Sieve Hollow Fiber Membranes. *Industrial & Engineering Chemistry Research* **2020**, *59*, 13755–13761.
- (6) Vu, D. Q.; Koros, W. J.; Miller, S. J. High Pressure CO₂/CH₄ Separation Using Carbon Molecular Sieve Hollow Fiber Membranes. *Industrial & Engineering Chemistry Research* **2002**, *41*, 367–380.
- (7) Kumar, R.; Zhang, C.; Itta, A. K.; Koros, W. J. Highly Permeable Carbon Molecular Sieve Membranes for Efficient CO₂/N₂ Separation At Ambient and Subambient Temperatures. *Journal of Membrane Science* **2019**, *583*, 9 – 15.
- (8) Rungta, M.; Wenz, G. B.; Zhang, C.; Xu, L.; Qiu, W.; Adams, J. S.; Koros, W. J. Carbon Molecular Sieve Structure Development and Membrane Performance Relationships. *Carbon* **2017**, *115*, 237–248.
- (9) Song, W.; Park, J.; Dasgupta, S.; Yao, C.; Maroli, N.; Behera, H.; Yin, X.; Acharya, D. P.; Zhang, X.; Doherty, C. M.; Maiti, P. K.; Freeman, B. D.; Kumar, M. Scalable Pillar[5]Arene-Integrated Poly(Arylate-Amide) Molecular Sieve Membranes To Separate Light Gases. *Chemistry of Materials* **2022**, *34*, 6559–6567.
- (10) Li, L.; Xu, R.; Song, C.; Zhang, B.; Liu, Q.; Wang, T. A review on the progress in nanoparticle/C hybrid CMS membranes for gas separation. *Membranes* **2018**, *8*, 134.

- (11) Williams, P. J. Analysis of Factors Influencing the Performance of Cms Membranes for Gas Separation. Ph.D. thesis, Georgia Institute of Technology, 2006.
- (12) Paul, D. The Solution-Diffusion Model for Swollen Membranes. *Separation and Purification Methods* **1976**, *5*, 33–50.
- (13) Wijmans, J. G.; Baker, R. W. The Solution-Diffusion Model: A Review. *Journal of Membrane Science* **1995**, *107*, 1–21.
- (14) Lonsdale, H. The Growth of Membrane Technology. *Journal of Membrane Science* **1982**, *10*, 81–181.
- (15) Suloff, E. Permeability, Diffusivity, and Solubility of Gas and Solute Through Polymers. *Sorption Behav. An Aliphatic Ser. Aldehydes Presence Poly (Ethylene Terephthalate) Blends Contain. Aldehyde Scav. Agents* **2002**, 29–99.
- (16) Skoulidas, A. I.; Sholl, D. S.; Johnson, J. K. Adsorption and Diffusion of Carbon Dioxide and Nitrogen Through Single-Walled Carbon Nanotube Membranes. *The Journal of Chemical Physics* **2006**, *124*, 054708.
- (17) Verploegh, R. J.; Nair, S.; Sholl, D. S. Temperature and Loading-Dependent Diffusion of Light Hydrocarbons in ZIF-8 as Predicted Through Fully Flexible Molecular Simulations. *Journal of the American Chemical Society* **2015**, *137*, 15760–15771, Pmid: 26606267.
- (18) Selassie, D.; Davis, D.; Dahlin, J.; Feise, E.; Haman, G.; Sholl, D. S.; Kohen, D. Atomistic Simulations of CO₂ and N₂ Diffusion in Silica Zeolites: The Impact of Pore Size and Shape. *The Journal of Physical Chemistry C* **2008**, *112*, 16521–16531.
- (19) Kamala, C. R.; Ayappa, K. G.; Yashonath, S. Mutual Diffusion in A Binary Ar-Kr Mixture Confined Within Zeolite Nay. *Phys. Rev. E* **2002**, *65*, 061202.
- (20) Kumar, N. A.; Gaddam, R. R.; Suresh, M.; Varanasi, S. R.; Yang, D.; Bhatia, S. K.; Zhao, X. Porphyrin–Graphene Oxide Frameworks for Long Life Sodium Ion Batteries. *J. Mater. Chem. A* **2017**, *5*, 13204–13211.
- (21) Thornton, A. W.; Nairn, K. M.; Hill, A. J.; Hill, J. M. New Relation Between Diffusion and Free Volume: I. Predicting Gas Diffusion. *Journal of Membrane Science* **2009**, *338*, 29–37.
- (22) Bousige, C.; Levitz, P.; Coasne, B. Bridging Scales in Disordered Porous Media by Mapping Molecular Dynamics Onto Intermittent Brownian Motion. *Nature Communications* **2021**, *12*, 1043.
- (23) Neyertz, S.; Brown, D. A Trajectory-Extending Kinetic Monte Carlo (Tekmc) Method for Estimating Penetrant Diffusion Coefficients in Molecular Dynamics Simulations of Glassy Polymers. *Macromolecules* **2010**, *43*, 9210–9214.

- (24) Neyertz, S.; Brown, D.; Pandiyan, S.; Van Der Vegt, N. F. Carbon Dioxide Diffusion and Plasticization in Fluorinated Polyimides. *Macromolecules* **2010**, *43*, 7813–7827.
- (25) Robeson, L. M. Correlation of Separation Factor Versus Permeability for Polymeric Membranes. *Journal of Membrane Science* **1991**, *62*, 165–185.
- (26) Freeman, B. D. Basis of Permeability/Selectivity Tradeoff Relations in Polymeric Gas Separation Membranes. *Macromolecules* **1999**, *32*, 375–380.
- (27) Robeson, L. M. The Upper Bound Revisited. *Journal of Membrane Science* **2008**, *320*, 390–400.
- (28) Robeson, L.; Freeman, B.; Paul, D.; Rowe, B. An Empirical Correlation of Gas Permeability and Permselectivity in Polymers and Its Theoretical Basis. *Journal of Membrane Science* **2009**, *341*, 178–185.
- (29) Comesaña-Gándara, B.; Chen, J.; Bezzu, C. G.; Carta, M.; Rose, I.; Ferrari, M.-C.; Esposito, E.; Fuoco, A.; Jansen, J. C.; Mckeown, N. B. Redefining the Robeson Upper Bounds for CO₂/CH₄ and CO₂/N₂ Separations Using A Series of Ultrapermeable Benzotriptycene-Based Polymers of Intrinsic Microporosity. *Energy Environ. Sci.* **2019**, *12*, 2733–2740.
- (30) Yang, Z.; Guo, W.; Mahurin, S. M.; Wang, S.; Chen, H.; Cheng, L.; Jie, K.; Meyer, H. M.; Jiang, D.-E.; Liu, G.; Jin, W.; Popovs, I.; Dai, S. Surpassing Robeson Upper Limit for CO₂/N₂ Separation With Fluorinated Carbon Molecular Sieve Membranes. *Chem* **2020**, *6*, 631–645.
- (31) Han, Y.; Ho, W. W. Polymeric Membranes for CO₂ Separation and Capture. *Journal of Membrane Science* **2021**, *628*, 119244.
- (32) Barnett, J. W.; Bilchak, C. R.; Wang, Y.; Benicewicz, B. C.; Murdock, L. A.; Bereau, T.; Kumar, S. K. Designing Exceptional Gas-Separation Polymer Membranes Using Machine Learning. *Science Advances* **2020**, *6*, Eaaz4301.
- (33) Li, H.; Zhang, X.; Chu, H.; Qi, G.; Ding, H.; Gao, X.; Meng, J. Molecular Simulation On Permeation Behavior of CH₄/CO₂/H₂S Mixture Gas in PvdF At Service Conditions. *Polymers* **2022**, *14*, 545.
- (34) Krishna, R. Diffusion of Binary Mixtures in Zeolites: Molecular Dynamics Simulations Versus Maxwell–Stefan Theory. *Chemical Physics Letters* **2000**, *326*, 477–484.
- (35) Bashir, M. A.; Al-Haj Ali, M.; Kanellopoulos, V.; Seppälä, J.; Kokko, E.; Vijay, S. The Effect of Pure Component Characteristic Parameters On Sanchez–Lacombe Equation-Of-State Predictive Capabilities. *Macromolecular Reaction Engineering* **2013**, *7*, 193–204.
- (36) Mahmood, S.; Xin, C.; Lee, J.; Park, C. Study of Volume Swelling and Interfacial Tension of the Polystyrene–Carbon Dioxide–Dimethyl Ether System. *Journal of Colloid and Interface Science* **2015**, *456*, 174–181.

- (37) Dasgupta, S.; M., R.; Roy, P. K.; foram M. Thakkar; Pathak, A. D.; Ayappa, K. G.; Maiti, P. K. Influence of Chain Length On Structural Properties of Carbon Molecular Sieving Membranes and Their Effects On CO₂, CH₄ and N₂ Adsorption: A Molecular Simulation Study. *Journal of Membrane Science* **2022**, *664*, 121044.
- (38) Roy, P. K.; Kumar, K.; Thakkar, f. M.; Pathak, A. D.; Ayappa, K. G.; Maiti, P. K. Investigations On 6fda/Bpda-Dam Polymer Melt Properties and CO₂ Adsorption Using Molecular Dynamics Simulations. *Journal of Membrane Science* **2020**, *613*, 118377.
- (39) Kiyono, M.; Williams, P. J.; Koros, W. J. Effect of Pyrolysis Atmosphere On Separation Performance of Carbon Molecular Sieve Membranes. *Journal of Membrane Science* **2010**, *359*, 2–10.
- (40) Potoff, J. J.; Siepmann, J. I. Vapor–Liquid Equilibria of Mixtures Containing Alkanes, Carbon Dioxide, and Nitrogen. *Aiche J.* **2001**, *47*, 1676–1682.
- (41) Mayo, S. L.; Olafson, B. D.; Goddard, W. A. Dreiding: A Generic force Field for Molecular Simulations. *Journal of Physical Chemistry* **1990**, *94*, 8897–8909.
- (42) Plimpton, S.; Crozier, P.; Thompson, A. Lammps-Large-Scale Atomic/Molecular Massively Parallel Simulator. *Sandia National Laboratories* **2007**, *18*, 43.
- (43) Tien, W.-J.; Chiu, C.-C. Generic Parameters of Trajectory-Extending Kinetic Monte Carlo for Calculating Diffusion Coefficients. *Aip Advances* **2018**, *8*, 065311.
- (44) Mark, P.; Nilsson, L. Structure and Dynamics of the Tip3p, Spc, and Spc/E Water Models At 298 K. *The Journal of Physical Chemistry A* **2001**, *105*, 9954–9960.
- (45) Tsimpanogiannis, I. N.; Moulton, O. A.; Franco, L. F. M.; de M. Spera, M. B.; Erdos, M.; Economou, I. G. Self-diffusion coefficient of bulk and confined water: a critical review of classical molecular simulation studies. *Molecular Simulation* **2019**, *45*, 425–453.
- (46) Alexander Stern, S. Polymers for Gas Separations: The Next Decade. *Journal of Membrane Science* **1994**, *94*, 1–65.
- (47) Peng, D.-Y.; Robinson, D. B. A New Two-Constant Equation of State. *Industrial & Engineering Chemistry Fundamentals* **1976**, *15*, 59–64.
- (48) Dubbeldam, D.; Calero, S.; Ellis, D. E.; Snurr, R. Q. Raspa: Molecular Simulation Software for Adsorption and Diffusion in Flexible Nanoporous Materials. *Molecular Simulation* **2016**, *42*, 81–101.
- (49) Steel, K. M.; Koros, W. J. An Investigation of the Effects of Pyrolysis Parameters On Gas Separation Properties of Carbon Materials. *Carbon* **2005**, *43*, 1843–1856.
- (50) Coudert, F.-X.; Jeffroy, M.; Fuchs, A. H.; Boutin, A.; Mellot-Draznieks, C. Thermodynamics of Guest-Induced Structural Transitions in Hybrid Organic–Inorganic Frameworks. *Journal of the American Chemical Society* **2008**, *130*, 14294–14302, Pmid: 18821758.

- (51) Kamala, C. R.; Ayappa, K. G.; Yashonath, S. Large Distinct Diffusivity in Binary Mixtures Confined To Zeolite Nay. *The Journal of Physical Chemistry B* **2005**, *109*, 22092–22095, Pmid: 16853874.
- (52) Baker, R. W.; Low, B. T. Gas Separation Membrane Materials: A Perspective. *Macromolecules* **2014**, *47*, 6999–7013.
- (53) Jamali, S. H.; Bardow, A.; Vlugt, T. J. H.; Moulton, O. A. Generalized Form for Finite-Size Corrections in Mutual Diffusion Coefficients of Multicomponent Mixtures Obtained from Equilibrium Molecular Dynamics Simulation. *Journal of Chemical Theory and Computation* **2020**, *16*, 3799–3806, PMID: 32338889.
- (54) Berendsen, H.; Grigera, J.; Straatsma, T. The Missing Term in Effective Pair Potentials. *Journal of Physical Chemistry* **1987**, *91*, 6269–6271.
- (55) Schneider, T.; Stoll, E. Molecular-Dynamics Study of A Three-Dimensional One-Component Model for Distortive Phase Transitions. *Physical Review B* **1978**, *17*, 1302.
- (56) NosÉ, S. A Unified formulation of the Constant Temperature Molecular Dynamics Methods. *The Journal of Chemical Physics* **1984**, *81*, 511–519.
- (57) Hoover, W. G. Canonical Dynamics: Equilibrium Phase-Space Distributions. *Physical Review A* **1985**, *31*, 1695.
- (58) Ryckaert, J.-P.; Ciccotti, G.; Berendsen, H. J. Numerical Integration of the Cartesian Equations of Motion of A System With Constraints: Molecular Dynamics of N-Alkanes. *Journal of Computational Physics* **1977**, *23*, 327–341.
- (59) Hockney, R. W.; Eastwood, J. W. *Computer Simulation Using Particles*; Crc Press, 2021.
- (60) Mills, R. Self-Diffusion in Normal and Heavy Water in the Range 1-45. Deg. *The Journal of Physical Chemistry* **1973**, *77*, 685–688.
- (61) Price, W. S.; Ide, H.; Arata, Y. Self-Diffusion of Supercooled Water To 238 K Using Pgs Nmr Diffusion Measurements. *The Journal of Physical Chemistry A* **1999**, *103*, 448–450.